Leveraging Tree Statistics for Extracting Anatomical Trees from 3D Medical Images

Mengliu Zhao, Brandon Miles and Ghassan Hamarneh
Medical Image Analysis Lab, School of Computing Science,
Simon Fraser University, Canada
{mengliuz, bmiles, hamarneh}@sfu.ca

***Abstract*—Using different priors (e.g. shape and appearance) have proven critical for robust image segmentation of different types of target objects. Many existing methods for extracting trees (e.g. vascular or airway trees) from medical images have leveraged appearance priors (e.g. tubular-ness and bifurcation-ness) and the knowledge of the cross-sectional geometry (e.g. circles or ellipses) of the tree-forming tubes. In this work, we present the first method for 3D tree extraction from 3D medical images (e.g. CT or MRI) that, in addition to appearance and cross-sectional geometry priors, utilizes prior tree statistics collected from the training data. Our tree extraction method collects and leverages topological tree prior and geometrical statistics, including tree hierarchy, branch angle and length statistics. Our implementation takes the form of a Bayesian tree centerline tracking method combining the aforementioned tree priors with observed image data. We evaluated our method on both synthetic 3D datasets and real clinical CT chest datasets. For synthetic data, our method's key feature of incorporating tree priors resulted in at least 13% increase in correctly detected branches under different noise levels. For real clinical scans, the mean distance from ground truth centerlines to the detected centerlines by our method was improved by 12% when utilizing tree priors. Both experiments validate that, by incorporating tree statistics, our tree extraction method becomes more robust to noise and provides more accurate branch localization.**

***Keywords*- segmentation; machine learning; statistical analysis; tree structure; centerline tracking;**

I. Introduction

Every year, millions of people are affected by circulatory and respiratory system problems. According to the World Health Organization, more than 3 million people died of chronic obstructive pulmonary disease (COPD) in 2012, which is equal to 6% of all deaths globally that year [1]. (Semi-)automatic tree structure segmentation from 3D images is important for both vasculature and airway analysis [2], diagnosis and pre-operative planning [3]. However, due to low contrast (especially in low-dose CT), similar attenuation coefficients (i.e., CT voxel values) of air and pulmonary parenchyma along with distorted tubular shapes (e.g., narrowed airways with COPD) and imaging artifacts, tree structure extraction becomes a challenging problem [4].

Many methods for segmenting tubular branching structures, such as airways and vasculature based on centerline tracking and machine learning have been proposed in recent years [4], but only a few were based on statistics and none of them utilized topological priors from an anatomical point of view, such as airway tree hierarchy, or geometrical statistics, such as branch angles and lengths, like we do in this work. We divide the existing literature on tree-extraction from 2D and 3D images into the following six main classes.

(i) Region Growing and Active Contour: Most of the airway extraction methods, mentioned in the comparative study paper of Lo *et al.* [5], were based on region growing, which makes it still hard to integrate statistical information like tubular geometry or airway morphometry. For example, Feuerstein *et al.* [6] proposed a region growing method to extract the airways using LoG enhanced images. Graham *et al.* first extracted the airways by region growing, then filtered the segmentation into small airway segments, and eventually removing spurious false airway tree branches by optimizing a graph-partitioning problem [7]. As for active contour methods, most still use information like the gradient and Hessian, and it's not obvious how to encode anatomical tree topology in these frameworks. Wang *et al.* [8] proposed to use 4D curves to extract tree structures, generalizing snake contours with cylinder models and propagated the front by gradient vector flow (GVF) force, the eigenvector of the Jacobian matrix and region intensity. Shang *et al.* [9] adopted a combined approach, first segmenting wider vessels by propagating the active contour front using intensity information, then segmenting smaller vessels with Hessian eigenvectors and eigenvalues and investigating the characteristics of principal curvatures.

(ii) Trackers: These methods are typically initialized with a seed at the root of the tree, then the tracker advances from this seed down through the tree. To explore different branches, these trackers either (a) explicitly locate bifurcations and split accordingly into children branch trackers [10], [11], [12], [13]; or (b) explore different possible paths thus implicitly defining tree bifurcations, e.g., the particle filtering based coronary vessel tracking method of Florin *et al.* [10]. A key computational module in such trackers is a search for the next point along the tree branch to advance to. This in turn typically requires two types of "regularization": The first is to regularize the path to avoid sudden abrupt turns by

the tracker, e.g., via Kalman filtering, as proposed in the 2D retinal blood vessel tracking method of Chutatape *et al.* [14]. The other is to regularize the data via image de-noising and tube (vesselness or ridge) filtering, as proposed by the 3D tracking method of Kumar *et al.* [15], [16].

(iii) Minimal Paths: Here each branch of a tree-like structure is one that "optimally" connects a pair of (start-end) points. Typically, manual seeding combined with image processing is used to detect likely start-end points. Optimality, on the other hand, is obtained using a potential map that is constructed based on image evidence, e.g. paths that pass through pixels with a strong vesselness (Frangi *et al.* [17]), are more favourable, as proposed by Soleimanifard *et al.* [18]. In their work, the energy functional satisfied the Eikonal equation and was optimized using level sets. In the work by Breitenreicher *et al.* [19] the potential map was based on extracting Haar features at different scales.

(iv) Machine Learning: This class of method relies on training machine learning systems to predict the class (or the probability of the class) of each pixel or voxel, where the two possible classes are tree (or branch) vs. background. Once the prediction map is obtained, different methods are used to join likely branch voxels into one contiguous tree segmentation. A voxel-wise classification method was proposed by Lo *et al.* [20], [21], in which they used a KNN classifier to first generate an airway probability map followed by vessel tracking using region growing. Probability Boosting Tree (PBT) classifier was used in [22] instead to obtain the coronary vessel paths. There are also other works proposing novel features [23], [24] for classifying bifurcations.

(v) Graph based methods: A graph based method was proposed in Bauer *et al.* [25], [26], detecting tube-like structures in the beginning and then connecting them into a tree graph. In the work of Hu *et al.* [27], graph-cut was performed locally in a neighboring sphere, segmenting vessel points by intensity differences. In [28], accurate airway wall extraction was obtained by an optimal graph construction method, which was based on an initial coarse airway segmentation provided by an algorithm proposed by Lo *et al.* [5].

(vi) Hybrid and others: Other methods which cannot be divided into the categories above include, for example, a differential geometry based method, proposed by Pu *et al.* [29], that filters airway regions by calculating principal curvature on isosurfaces. Tree structure optimization was performed in the work of Zhu *et al.* [30], but the optimization only prunes spurious branches and breaks loops, rather than using hierarchical information. Aside from segmentation purposes, there are existing works investigating tree statistics extracted from binary segmentation results [31], [32].

Although in some of the works mentioned above, statistical methods like Bayesian inference were applied, as in the work of Wang *et al.* [11], no tree statistics were actually used. In the work of Florin *et al.* [10], the inference rule was simply applied on inferring parameters from the last tracking step, so no global statistical information was embedded. On the other hand, topological information like branching types (in mice airways) has been analyzed in the work of Grothausmann *et al.* [33], however, the aim of their work is not about airway extraction and the information extracted is yet unknown how to further help in airway (human's, especially) segmentation. In general, our key contribution in this paper is fully utilizing tree topology information and geometrical statistics to aid the segmentation process, while none of the methods surveyed have explored.

Tree-like structures in living beings, like the Circle of Willis in the brain, the airways in the lung and the abdominal arteries (Figure 1), are not perfectly identical across a population. Nevertheless, these trees conform to particular topological and geometrical patterns largely consistent across the normal (non-pathological) adult population. In particular, the first several generations of branching (e.g. root, first two children, the four grandchildren) are known to respect a well-defined hierarchy, which our approach is designed to leverage.

In this paper, we propose a new tree tracking method that incorporates, not only image features (or appearance priors), but also, and for the first time, geometrical and topological tree priors to improve tracking and bifurcation detection of tree-structures in 3D medical images (such as magnetic resonance imaging, MRI, or computed tomography, CT). The geometrical priors include branch length and angle statistics, which are learnt from segmented training images. Our tracker conforms to a topological prior (i.e. branching pattern, Figure 1), that enables leveraging the appropriate branch- and level-specific geometrical statistics. For example, the trachea always branches into left and right main bronchi, while left main bronchus further develops into superior and inferior lobar bronchus, and right main bronchus into superior and intermediate lobar bronchus. We implement our method by adopting a Bayesian formulation that incorporates the aforementioned tree-priors. Quantitative and qualitative results show that by using geometrical and topological priors, the accuracy and stability of tree extraction is significantly improved.

II. Method

A. Tree Extraction with Tree Priors

At a high level, we adopt a Bayesian formulation to infer bifurcation locations while tracking tree centerlines, with given topological and geometrical priors. The proposed tracker works by continually advancing through the image to map the airway/vessel centerlines, and bifurcating when a branching point is detected. Branch length statistics play the important role of weighting the probability to bifurcate, which is inferred from the image features (i.e., the likelihood), by probabilities inferred from the geometrical priors, via Bayes' theorem. Branch angle statistics further

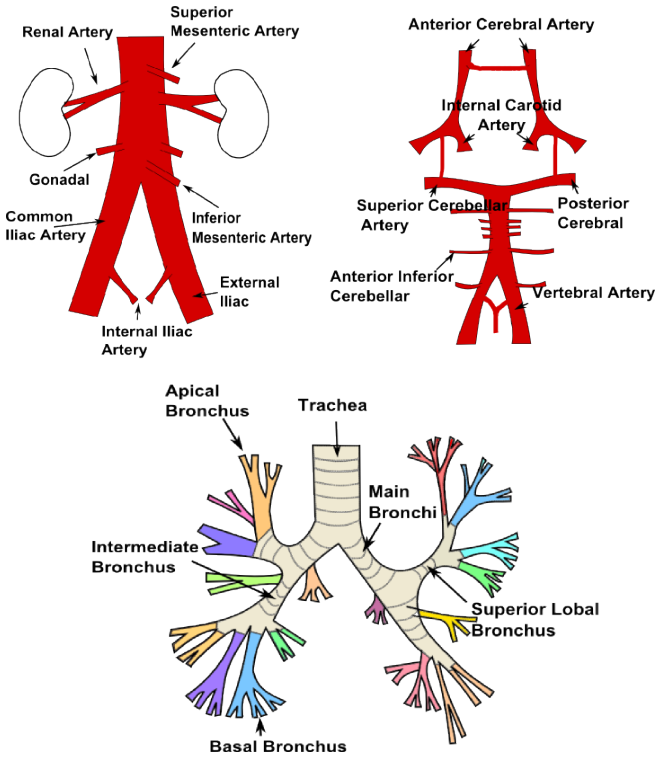

Figure 1: Different examples of tree structures in human anatomy: Upper left: Abdominal aorta; Upper right: Circle of Willis; Bottom: Bronchial tree.

help to locate daughter branches by giving lower penalties to branching directions that agree with angular priors. The tree topology, on the other hand, is embedded as follows: As our tracker progresses from the tree root downward along the branches into 3D images, we continuously update a tree data structure with a crawler pointer or tag indicating where on the tree model our tracker is, which branch (trachea, right main bronchi, ...) or at which level (level 1, 2, 3, ...) is currently actively being tracked. This allows us to pull the corresponding level- and branch-specific geometrical priors.

To extract the full tree, a key decision of where, down along a each tracked branch, the tracker must bifurcate (e.g. where to bifurcate the root into children, or the each child into grandchildren). Additionally, once the decision to bifurcate is made, the initial tracking directions of the two child branches must be resolved. The next two sections focus on describing the details of these key modules.

B. Bifurcation Classification Criterion

We denote B_i as the occurrence of bifurcation at the tree level i, I the image features, L_i the random variable representing the detected branch length, and l the prior level- and branch-specific length value. We assume I and L_i are independent, since branch length is a global geometrical property, while the image features are locally defined. $P(I)$ and $P(L_i \leq l)$ are prior distributions, since they are not relevant to B_i, they could be replaced by constant values here. We also assume $P(I|B_i)$ to be of uniform distribution. Thus, the probability of finding a bifurcation at tree level i with detected branch length L_i is as follows:

$$\begin{aligned} P(B_i|I, L_i \leq l_i) &= \frac{P(B_i)P(L_i \leq l_i, I|B_i)}{P(L_i \leq l_i, I)} \\ &= C' \frac{P(B_i|I)P(I)P(L_i \leq l|B_i)P(I|B_i)}{P(L_i \leq l_i, I)} \\ &= CP(L_i \leq l_i|B_i)P(B_i|I). \end{aligned} \tag{1}$$

The probability map $P(B_i|I)$ could be generated by a general bifurcation detection classifier. $P(L_i = l|B_i)$ can be collected from training data or based on expert knowledge of anatomy (see section III-A) and $P(L_i \leq l|B_i)$ is its cumulative density function (CDF). If we define weight $\omega = CP(L_i \leq l|B_i)$, C is some constant, then:

$$P(B_i|I, L_i \leq l_i) = \omega P(B_i|I). \tag{2}$$

The intuition behind Equation (2) is that, when the tracked branch length is much shorter than the mean length, it is less likely to have a bifurcation detected ($\omega < 1$); but as the length of the tracked branch exceeds the mean length, the probability of finding a bifurcation will increase nonlinearly (up to the scale C ($C > 1$), since we expect a bifurcation will eventually be found unless an end point is reached).

See Figure 2 as an example of where, $\omega \geq 1$ after reaching mean branch length $l = 60$ and is non-linearly increasing (at a rate dependent on the standard deviation, 15, in this case).

C. Daughter Branches Detection Criteria

The *probability* $P \in [0, 1]$ of bifurcating, given image evidence and prior level- and branch-specific lengths, calculated in section 2.2, will now be converted to a *decision* to bifurcate. One naïve approach is to bifurcate whenever $P > 0.5$. However, this approach does not take into account any evidence whether this candidate location x_0 for a bifurcation will result in two plausible child branches. To determine whether two branches can be identified at x_0, we follow the following procedure that leverages the branch angular statistics (Figure 3).

1) Denote the parent branch direction at x_0 as $\vec{p}$. First threshold the neighboring points so that any point y behind x_0 is discarded. This is computed by checking whether $\cos(< y - x_0, \vec{p} >) \leq 0$.
2) Denote the mean direction and standard deviation of each daughter branch as $\vec{\mu_i}$ and $\vec{\theta_i}$ (training of $\vec{\mu_i}$ and $\vec{\theta_i}$ is found in section III-A), respectively for branches $i = 1, 2$. Then threshold the neighboring points to be within 3 standard deviations θ (99.7% confidence

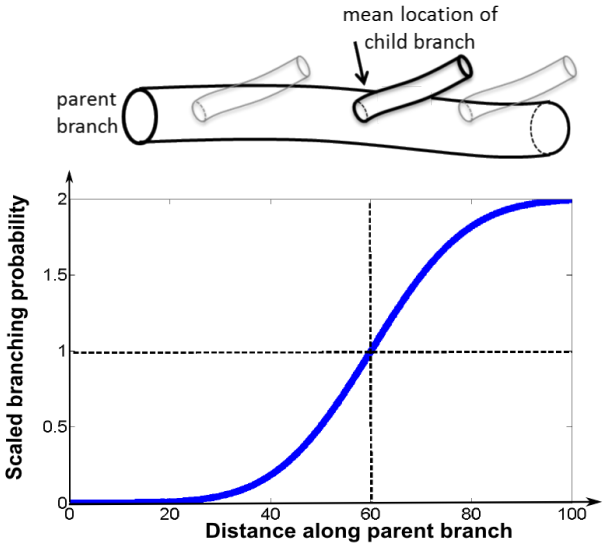

Figure 2: Probability of a parent branch to bifurcate given prior distribution of the parent branch length. Branching weight $\omega = CP(L_i \leq l|B_i)$ (as in Equation 2) increase according to branch length, where $C = 2$, $P(L_i \leq l|B_i)$ is Gaussian cumulative density function, given mean branch length $l = 60$, standard deviation 15.

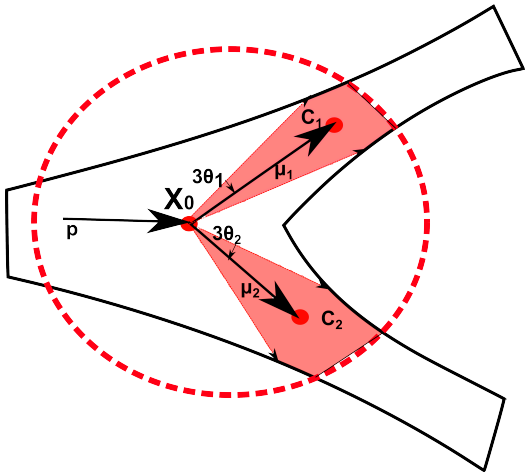

Figure 3: Illustration of daughter branches detection using angle statistics. p is the current branch direction. The red dashed circle is the neighborhood of X_0 (current search point). μ_1 and μ_2 are prior mean daughter directions, θ_1 and θ_2 their respective standard deviations. The pink areas are filtered neighboring points; any point outside will be discarded. C_1 and C_2 are the resulting clustered centroids that act as roots for tracking the daughter branches.

interval) of the daughter branch angles. This is done by checking:

$$\begin{aligned} \cos\left(\mu_i + \vec{} 3\theta_i\right) &\leq \cos\left(< y - x_0, \vec{p} >\right) \\ \cos\left(\mu_i - \vec{} 3\theta_i\right) &\geq \cos\left(< y - x_0, \vec{p} >\right), i = 1, 2. \end{aligned} \tag{3}$$

If the criterion in Equation (4) is satisfied, point y is kept; otherwise y is discarded (Figure 3).

3) The remaining neighboring points are clustered into two parts using k-means.
   a) If at least one cluster is empty, then the current point x_0 is rejected as a bifurcation, since we can't find its two daughter branches. The tracker will keep tracking the centerline of the current branch.
   b) Otherwise, there are two cluster centroids $c_i, i = 1, 2$. Then we check if the following two criteria are satisfied:
      i) mean image intensity along the path x_0 and c_i is within the given intensity threshold;
      ii) mean image intensity along the path c_1 and c_2 is beyond the intensity threshold, indicating there is a clear separation between the daughter branches.

   If both criteria above are satisfied, then x_0 is accepted a bifurcation and c_1, c_2 will be set as starting points of tracking the daughter branches.

III. Experimental Results

A. Description of the datasets

Synthetic Data: We generated 330 binary volumes, each of size 256*256*256 and containing a binary tree structure with 4 levels. The tree statistics are illustrated in Figure 4 and include: mean and standard deviation (std) of branch lengths that describe $P(L_i = l|B_i)$, as well as mean angles $\vec{\mu_i}$, and angle standard deviation (std) ($\vec{\theta_i}$ in section II-C), all assuming Gaussian distribution (it's worth to note the trees are not symmetric). Spatially-variant Gaussian noise was added to approximate low-dose CT acquisition [34], with standard deviation $\gamma * e^{0.5(f+1)}/3$ (so that std is nonlinearly proportional to image intensity and std ≤ 1 when $\gamma \leq 1$), where f is image intensity, and different noise levels $\gamma \in \{0.6, 0.8, 1.0\}$ (Figure 5).

Clinical Data: The clinical dataset was obtained from the 2009 MICCAI challenge [35], [36]. We used all 16 ground truth segmentation results provided by the organizers to generate ground truth centerlines by running the fast marching algorithm [37], [38], [39], and then calculate length and angle priors from these centerlines. Seven branches: trachea, right main bronchi (RMB), left main bronchi (LMB), right superior lobar bronchus (RSB), right intermediate bronchus (RIMB), left superior lobar bronchus (LSB) and left inferior lobar bronchus (LIFB) were manually labeled by a graduate student. See branch and angle statistics in Table I and Figure 6.

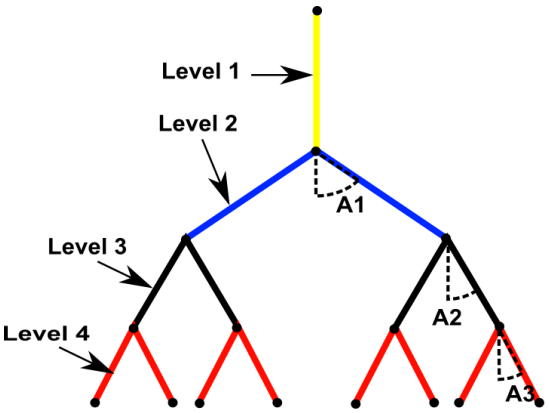

	Level 1	Level 2	Level 3	Level 4
mean	80	60	40	30
std	5	5	5	5

	Angle 1	Angle 2	Angle 3
mean	45°	45°	30°
std	5°	5°	5°

Figure 4: Top: Tree structure in a synthetic data; Middle rows: Statistics of branch lengths; Bottom rows: Statistics of angles.

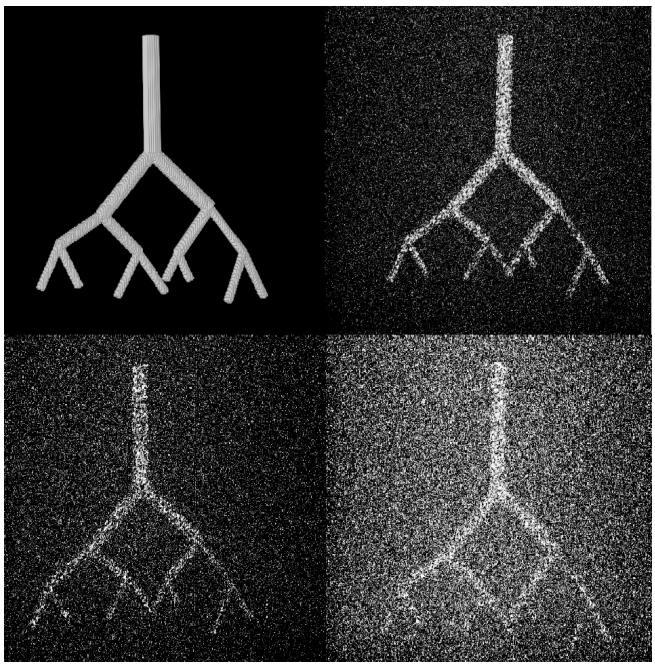

Figure 5: Synthetic 3D data with noise. Noise level from left to right, top to bottom: 0, 0.6, 0.8, 1.0.

	Level 1	Level 2	
	Trachea	RMB	LMB
mean length	**133.29**	**51.16**	**75.75**
min length	83.28	26.63	35.98
max length	208.01	97.00	103.49
std length	**36.40**	**19.32**	**18.61**
	Level 3			
	RSB	RIMB	LSB	LIFB
mean length	**30.41**	**33.17**	**24.73**	**47.58**
min length	21.49	13.00	10.95	15.00
max length	56.61	49.00	44.57	99.00
std length	**9.59**	**10.62**	**8.81**	**20.51**

Table I: Length statistics (in units of voxels) of real data.

B. Preprocessing and Initialization

In this paper, we manually set the starting point for the tracker in the synthetic data experiment. For the clinical data experiment, we adopt an approach similar to [40], [41], selecting a region of interest (ROI) by first choosing the uppermost 3/4 slices and a 256*256 square region in the center of each slice. The volume is then filtered by a 5*5 median filter on each slice. The 30th slice counting from the top is used for detecting the seed point. By detecting dark circles of radii between [5, 50] pixels, we choose the one closest to the center of the slice as the seed point.

C. Testing Results

Synthetic Data: Performance on the synthetic data was measured based on the number of detected branches not leaking into background regions. The results are summarized in Table II, which show that, even as the noise level increases from 0.6 to 1.0, the overall performance using statistical priors shows a steady improvement of at least 13% with statistics.

Noise Level	0.6	0.8	1.0
WOS	976	948	878
WS	**1250**	**1200**	**1000**
Improvement	**28.69%**	**26.58%**	**13.90%**

Table II: Number of branches detected in synthetic data. WOS: method without statistics. WS: method using statistics.

Clinical Data: Evaluation was performed using leave-one-out cross-validation. Accuracy was measured by calcu-

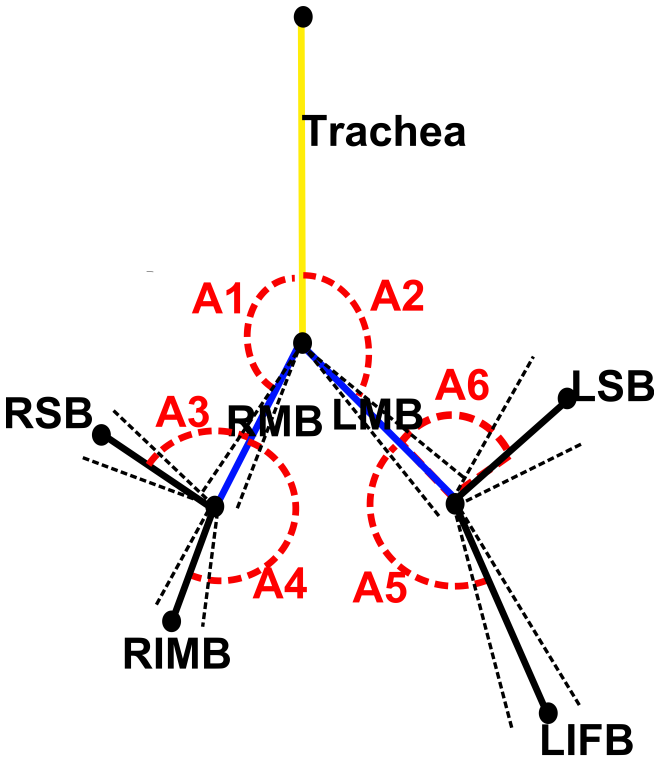

	A1	A2	A3
mean	144.71°	128.71°	97.01°
std	7.94°	9.82°	17.16°
	A4	A5	A6
mean	168.86°	158.16°	106.77°
std	5.79°	20.30°	9.54°

Figure 6: Angle statistics (in degrees) of real data. Top: Trachea is labeled in yellow, RMB and LMB are labeled in blue, the rest are labeled in black; all the mean angles are labeled in red dashed arcs; dashed black lines represent standard deviations. Bottom: Angle statistics.

lating the shortest Euclidean distances from the centerlines of the given ground truth segmentations (i.e. ground truth centerlines) to the detected centerlines. Qualitative results in Figure 7 show improved bifurcation detection and tree topology representation when using tree statistics. Quantitative results in Table III show that the mean distance from ground truth centerlines to detected centerlines (i.e. the error) is reduced by 12% by adding statistical priors. By running a paired t-test, we show that the result is of statistical significance with $p \leq 0.05$. Overall, we noted that by adding statistic priors, the tracking accuracy is significantly improved.

In both synthetic and clinical data experiments, we replace $P(B_i|I)$ in equation 2 by the Random Forest classifier as described in [24] with the same image features. The classifier is trained on synthetic samples in the synthetic data experiment and on real samples in the clinical data experiment.

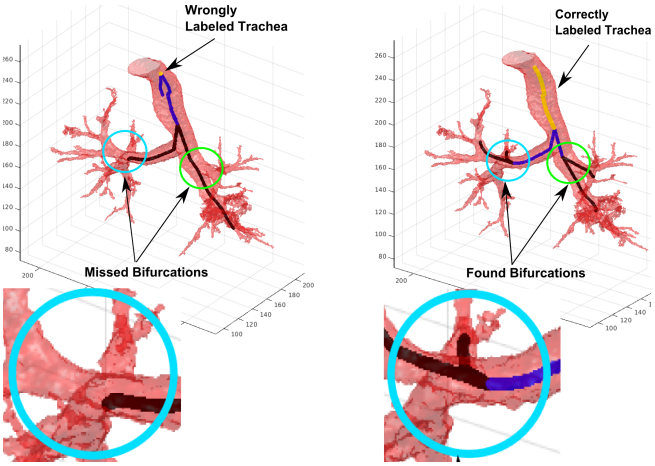

Figure 7: Centerline detected in real data. The pink surface is the binary segmentation of the volumes provided by the EXACT challenge. The yellow centerline corresponds to trachea (1st level), blue centerlines correspond to RMB and LMB (2nd level) and black centerlines correspond to RSB, RIMB, LSB and LIFB (3rd level). Figures in the bottom row are the zoomed-in cyan regions in the top row. Note the missing bifurcation highlighted by cyan and green circles in the left vs. properly detected in the right.

	Mean Distance	Standard Deviation
WOS	10.49	20.06
WS	**9.36**	**19.46**
Improvement	**12.07%**	**3.08%**

Table III: Distance (in units of voxels) from ground truth centerline in real clinical data to detected centerlines. WOS: method without statistics. WS: method using statistics. The improvement is of statistical significance with $p \leq 0.05$.

IV. Conclusion

In this work, we presented the first method in the medical image analysis field that incorporates prior and statistics of anatomical trees into a tree extraction algorithm. We developed a Bayesian based algorithm for tracking tree centerlines, utilizing statistical geometry priors as well as tree topology priors (including tree hierarchy, branch angle and

length statistics). By testing on synthetic images of different noise levels and real CT chest scans, the proposed method showed a clear improvement in terms of both stability and accuracy. This is supported in our experiments over real clinical data. While in our diagrams (e.g., Figure 4 and 6) and the results, we adopted a binary tree representation (containing only bifurcations), known to constitute the majority of real anatomical branchings patterns, our approach could be naturally extended to trees with trifurcations and more generations (levels) of branching. Future works will involve training and applying our method to tree-like vasculature with other tree topologies, such as the Circle of Willis in the brain to highlight areas of pathology, e.g. aneurysms. A possible weakness of our approach is that the tracking is limited by the adoption of a myopic, local decision making process; a multi-hypothesis extension, allowing the tracker to explore different paths, may yield further robustness to noise.

Acknowledgements Partial funding for this research was provided by the National Science and Engineering Research Council (NSERC) of Canada.

REFERENCES

[1] "World health organization fact sheet N315," 2015. [Online]. Available: www.who.int/mediacentre/factsheets/fs315/en/ 1

[2] A. Feragen, P. Lo, V. Gorbunova, M. Nielsen, A. Dirksen, J. Reinhardt, F. Lauze, and M. Bruijne, "An airway tree-shape model for geodesic airway branch labeling," in *Third International Workshop on Mathematical Foundations of Computational Anatomy*, 2011. 1

[3] M. Merkx, A. Bode, W. Huberts, J. Bescos, J. Tordoir, M. Breeuwer, V. F. de, and E. Bosboom, "Assisting vascular access surgery planning for hemodialysis by using MR, image segmentation techniques, and computer simulations," *Medical Biological Engineering Computing*, vol. 51, no. 8, pp. 879–889, 2013. 1

[4] J. Pu, S. Gu, S. Liu, S. Zhu, D. Wilson, J. Siegfried, and D. Gur, "CT based computerized identification and analysis of human airways: A review," *Medical Physics*, vol. 39, no. 5, pp. 2603–2616, 2012. 1

[5] P. Lo, J. Sporring, J. Pedersen, and M. de Bruijne, "Airway tree extraction with locally optimal paths," in *MICCAI*, 2009, vol. 5762, pp. 51–58. 1, 2

[6] M. Feuerstein, T. Kitasaka, and K. Mori, "Adaptive branch tracing and image sharpening for airway tree extraction in 3-D chest CT," in *Proc. of Second International Workshop on Pulmonary Image Analysis*, 2009. 1

[7] M. Graham, J. Gibbs, and W. Higgins, "Robust system for human airway-tree segmentation," in *SPIE*, 2008, vol. 6914, pp. 69 141J–69 141J–18. 1

[8] Y. Wang, A. Narayanaswamy, and B. Roysam, "Novel 4-D open-curve active contour and curve completion approach for automated tree structure extraction," in *CVPR*, 2011, pp. 1105–1112. 1

[9] Y. Shang, R. Deklerck, E. Nyssen, A. Markova, J. De Mey, X. Yang, and K. Sun, "Vascular active contour for vessel tree segmentation," *IEEE Transactions on Biomedical Engineering*, vol. 58, no. 4, pp. 1023–1032, 2011. 1

[10] C. Florin, N. Paragios, and J. Williams, "Particle filters, a quasi-monte carlo solution for segmentation of coronaries," in *MICCAI*, 2005, vol. 3749, pp. 246–253. 1, 2

[11] X. Wang, T. Heimann, P. Lo, M. Sumkauskaite, M. Puderbach, M. de Bruijne, H. Meinzer, and I. Wegner, "Statistical tracking of tree-like tubular structures with efficient branching detection in 3D medical image data," *Physics in Medicine and Biology*, vol. 57, no. 16, p. 5325, 2012. 1, 2

[12] S. Cetin, A. Demir, A. Yezzi, M. Degertekin, and G. Unal, "Vessel tractography using an intensity based tensor model with branch detection," *IEEE Transactions on Medical Imaging*, vol. 32, no. 2, pp. 348–363, 2013. 1

[13] C. McIntosh and G. Hamarneh, "Vessel crawlers: 3D physically-based deformable organisms for vasculature segmentation and analysis," in *CVPR*, vol. 1, 2006, pp. 1084–1091. 1

[14] O. Chutatape, L. Zheng, and S. Krishnan, "Retinal blood vessel detection and tracking by matched gaussian and kalman filters," in *Proceedings of the 20th Annual International Conference of the IEEE Engineering in Medicine and Biology Society*, vol. 6, 1998, pp. 3144–3149. 2

[15] R. Kumar, F. Albregtsen, M. Reimers, T. Lang, B. Edwin, and O. Elle, "3D multiscale vessel enhancement based centerline extraction of blood vessels," in *SPIE*, vol. 8669, 2013, pp. 86 691X–86 691X–9. 2

[16] R. Kumar, F. Albregtsen, M. Reimers, B. Edwin, T. Lang, and O. Elle, "Three-dimensional blood vessel segmentation and centerline extraction based on two-dimensional cross-section analysis," *Annals of Biomedical Engineering*, vol. 43, no. 5, pp. 1223–1234, 2015. 2

[17] A. Frangi, W. Niessen, K. Vincken, and M. Viergever, "Multiscale vessel enhancement filtering," in *MICCAI*, 1998, vol. 1496, pp. 130–137. 2

[18] S. Soleimanifard, M. Schar, A. Hays, R. Weiss, M. Stuber, and J. Prince, "Vessel centerline tracking and boundary segmentation in coronary MRA with minimal manual interaction," in *ISBI*, 2012, pp. 1417–1420. 2

[19] D. Breitenreicher, M. Sofka, S. Britzen, and S. Zhou, "Hierarchical discriminative framework for detecting tubular structures in 3D images," in *Information Processing in Medical Imaging*, 2013, vol. 7917, pp. 328–339. 2

[20] P. Lo, J. Sporring, and M. Bruijne, "Multiscale vessel-guided airway tree," *Medical Image Analysis*, vol. 14, no. 4, pp. 527–538, 2009. 2

[21] P. Lo, J. Sporring, H. Ashraf, J. Pedersen, and M. de Bruijne, "Vessel-guided airway tree segmentation: A voxel classification approach," *Medical Image Analysis*, vol. 14, no. 4, pp. 527 – 538, 2010. 2

[22] Y. Zheng, M. Loziczonek, B. Georgescu, S. Zhou, F. Vega-Higuera, and D. Comaniciu, "Machine learning based vesselness measurement for coronary artery segmentation in cardiac CT volumes," in *SPIE*, vol. 7962, 2011, pp. 79 621K–79 621K–12. 2

[23] J. Zhou, S. Chang, D. Metaxas, and L. Axel, "Vascular structure segmentation and bifurcation detection," in *ISBI*, 2007, pp. 872–875. 2

[24] M. Zhao and G. Hamarneh, "Bifurcation detection in 3D vascular images using novel features and random forest," in *ISBI*, 2014, pp. 421–424. 2, 6

[25] C. Bauer, "Segmentation of 3D tubular tree structures in medical images," Ph.D. dissertation, Graz University of Technology, 2010. 2

[26] C. Bauer, T. Pock, H. Bischof, and R. Beichel, "Airway tree reconstruction based on tube detection," in *Proc. of Second International Workshop on Pulmonary Image Analysis*, 2009, pp. 203–213. 2

[27] X. Hu and Y. Cheng, "Centerline-based vessel segmentation using graph cuts," in *Sixth International Conference on Graphic and Image Processing*, 2015, pp. 94 432E–94 432E. 2

[28] J. Petersen, M. Nielsen, P. Lo, Z. Saghir, A. Dirksen, and M. de Bruijne, "Optimal graph based segmentation using flow lines with application to airway wall segmentation," in *Information Processing in Medical Imaging*, 2011, vol. 6801, pp. 49–60. 2

[29] J. Pu, C. Fuhrman, W. Good, F. Sciurba, and D. Gur, "A differential geometric approach to automated segmentation of human airway tree," *IEEE Transactions on Medical Imaging*, vol. 30, no. 2, pp. 266–278, 2011. 2

[30] W. Zhu, B. Li, L. Tian, X. Li, and Q. Chen, "Topology adaptive vessel network skeleton extraction with novel medialness measuring function," *Computers in Biology and Medicine*, vol. 64, pp. 40 – 61, 2015. 2

[31] N. Amenta, M. Datar, A. Dirksen, M. de Bruijne, A. Feragen, X. Ge, J. Pedersen, M. Howard, M. Owen, J. Petersen, J. Shi, and Q. Xu, "Quantification and visualization of variation in anatomical trees," *arXiv:1410.2466*, 2014. 2

[32] A. Feragen, P. Lo, M. de Bruijne, M. Nielsen, and F. Lauze, "Toward a theory of statistical tree-shape analysis," *IEEE Transactions on Pattern Analysis and Machine Intelligence*, vol. 35, no. 8, pp. 2008–2021, 2013. 2

[33] R. Grothausmann, M. Kellner, M. Heidrich, R. Lorbeer, T. Ripken, H. Meyer, M. Kuehnel, M. Ochs, and B. Rosenhahn, "Method for 3D airway topology extraction," *Computational and Mathematical Methods in Medicine*, 2015. 2

[34] H. Lu, X. Li, I. Hsiao, and Z. Liang, "Analytical noise treatment for low-dose CT projection data by penalized weighted least-square smoothing in the K-L domain," in *SPIE*, vol. 4682, 2002, pp. 146–152. 4

[35] P. Lo, B. van Ginneken, J. Reinhardt, T. Yavarna, P. de Jong, B. Irving, C. Fetita, M. Ortner, R. Pinho, J. Sijbers, M. Feuerstein, A. Fabijanska, C. Bauer, R. Beichel, C. Mendoza, R. Wiemker, J. Lee, A. Reeves, S. Born, O. Weinheimer, E. van Rikxoort, J. Tschirren, K. Mori, B. Odry, D. Naidich, I. Hartmann, E. Hoffman, M. Prokop, J. Pedersen, and M. de Bruijne, "Extraction of airways from CT (EXACT'09)," *IEEE Transactions on Medical Imaging*, vol. 31, no. 11, pp. 2093–2107, 2012. 4

[36] "EXACT'09 challenge," Online, 2009. [Online]. Available: http://image.diku.dk/exact/index.php 4

[37] R. Van Uitert and I. Bitter, "Subvoxel precise skeletons of volumetric data based on fast marching methods," *Medical Physics*, vol. 34, no. 2, pp. 627–638, 2007. 4

[38] M. Hassouna and A. Farag, "Multistencils fast marching methods: A highly accurate solution to the eikonal equation on cartesian domains," *IEEE Transactions on Pattern Analysis and Machine Intelligence*, vol. 29, no. 9, 2007. 4

[39] J. Bærentzen, "On the implementation of fast marching methods for 3D lattices," Tech. Rep., 2001. 4

[40] J. Lee and A. Reeves, "Segmentation of the airway tree from chest CT using local volume of interest," in *Proc. of Second International Workshop on Pulmonary Image Analysis*, 2009, pp. 273–284. 5

[41] O. Weinheimer, T. Achenbach, and C. Düber, "Fully automated extraction of airways from CT scans based on self-adapting region growing," *Computerized Tomography*, vol. 27, no. 1, pp. 64–74, 2008. 5